World Scientific
www.worldscientific.com

A higher order slip flow of generalized Micropolar nanofluid with applications of motile microorganisms, nonlinear thermal radiation and activation energy

Usman,* M. Ijaz Khan†, Sami Ullah Khan‡, Abuzar Ghaffari§, Yu-Ming Chu¶,‖,**
and Shahid Farooq†

*Beijing Key Laboratory for Magneto-Photoelectrical Composite and Interface Science,
Department of Applied Mathematics, School of Mathematics and Physics,
University of Science and Technology Beijing, Beijing 100083, P. R. China
†Department of Mathematics and Statistics, Riphah International University,
I-14, Islamabad 44000, Pakistan
‡Department of Mathematics, COMSATS University Islamabad,
Sahiwal 57000, Pakistan
§Department of Mathematics, University of Education,
Lahore (Attock Campus 43600), Pakistan
¶Department of Mathematics, Huzhou University, Huzhou 313000, P. R. China
‖Hunan Provincial Key Laboratory of Mathematical Modeling and Analysis in Engineering,
Changsha University of Science and Technology, Changsha 410114, P. R. China
**chuyuming@zjhu.edu.cn

This communication aims to develop the thermal flow model for generalized micropolar nanofluid with insensitive applications of bioconvection, activation energy and nonlinear thermal radiation. The generalized micropolar fluid model is the extension of traditional micropolar fluid model with viscoelastic relations. The viscous nature of non-Newtonian micropolar material can be successfully predicted with help of this model. The motivating idea for considering the motile microorganisms is to control the nanoparticles suspension effectively. The higher order slip relations are incorporated to examine the bio-convective phenomenon. The simplified coupled equations in terms of non-dimensional variables are numerically treated with shooting scheme. The reliable graphical outcomes are presented for flow parameters governed to the transported problem. The flow pattern of each parameter is highlighted in view of viscous nature of micropolar fluid.

Keywords: Generalized micropolar nanofluid; higher order slip; motile microorganisms; nonlinear thermal radiation; shooting technique.

PACS number: 83.50.Ha

**Corresponding author.

1. Introduction

The research in nanofluid presents a growing interest of researchers due to their multidisciplinary applications in heat exchangers, heating processes, cooling systems, aerospace technology, heating devices, microelectronics sectors, fuel processing, etc. Owing to the nanotechnology revolution, the nanoparticles are considered as an effective heat enhancement mechanism with nanoscale (1–100 nm). The base materials efficiencies achieve a remarkable trend due to suspension of nanoparticles. The heat transportation and absorbing characteristics of working liquids are improved by utilizing the nanofluids. The deviated and ultra-high performances of nanofluids developed considerable interest in recent days. Choi[1] presented first attention on the classical idea of nanofluids supported with experimental observations. Buongiorno[2] specified the slip mechanism of Brownian and thermophoretic prospective for nanofluids. Bhatti *et al.*[3] explored the thermal improvement of base fluid with interaction of Fe_3O_4 tiny sized particles accounting thermal radiation effects and diffusion applications. Sohail and Raza[4] used the control mass flux constraints for exploring the pseudo-plastic type non-Newtonian materials with nanofluid immersion. Khan *et al.*[5] examined the activation energy applications in tangent hyperbolic nanofluid supported with joint features of magnetic and electric forces. Moreover, the flow has been controlled by imposing slip relations of higher order at the moving surface. The stability assessment of hybrid nanofluids along with the work of dual solutions encountered by shrinked/stretched surfaces has been reported numerically by Lund *et al.*[6] Turkyilmazoglu[7] worked out the linear stability inspection while exploring the thermal mechanism of nanofluid based on single model relations. The research reported by Oudina *et al.*[8] examined the importance of discrete heat source in nanoliquids confined by vertical cylinder for which walls are suggested to be porous. Kumar *et al.*[9] assumed the viscoelastic nanofluid between two expanding and squeezing surfaces in order to notice the thermal properties. The entropy generation exploration and involvement of activation energy in nanofluids configured by curved surfaces was focused analytically by Khan *et al.*[10] Chu *et al.*[11] focused on the optimized flow of second grade nanofluid with modified diffusion relations and variable thermal properties.

The bioconvection pattern appeared when the microorganisms move in the upward direction in the flow configuration. This upward motion of microorganisms results the appearance of heavy bacteria layer in the top surface *f* lighter liquid. It is commonly observed that unstable situation created when density of bacteria becomes extremely higher and subsequently the bacterial layers shattered in colony of convection cells. The concept of bioconvection is associated with the joined features of buoyancy forces, microorganisms and density stratification. The microorganisms are characterized into gyrotaxis, oxytaxis and gravitaxis. Upon addition of microorganisms in nanofluids, the stability of nanomaterials improved up to an impressive level. The pioneer research which examines the bioconvection aspect of nanofluids has been done by Kuznetsov.[12,13] Recently, many investigations are addressed in the

dynamic literature which accesses the mechanism of nanofluids along with motile microorganisms. Zohra *et al.*[14] introduced a new type of slip relations (anisotropic slip) to address the bioconvection prospective of nanofluid truncated in rotating cone and subject to the Stefan and blowing constrains. Atif *et al.*[15] visualized the dynamic of micropolar nanofluid with gyrotactic microorganisms. The study and role of magnetic Reynolds number on the bio-convective flow of nanofluid assumed between circular plates was explored by Zhang *et al.*[16] Khan *et al.*[17] conducted thermal study on flow of Oldroyd-B nanofluid which contains gyrotactic microorganisms theoretically. The significances oxytactic microorganisms in nanofluids of rotational type with utilization of convective conditions were directed by Dhlamini *et al.*[18] Zeeshan *et al.*[19] discussed the two-dimensional (2D) flow pattern of couple stress nanofluid confined by paraboloid revolution. Waqas *et al.*[20] numerically tackled the bioconvection problem of nanofluid along with the relations of activation energy and viscous dissipation. Aldabesh *et al.*[21] intended the transient slip flow of Williamson nanofluid with applications of bioconvection phenomenon and slip effects. Waqas *et al.*[22] examined thermally developed analysis for the nanomaterials in presence of gyrotactic microorganisms.

With analogous features and complicated behavior of non-Newtonian materials, a variety of research has been performed on this topic and popular in the researchers even current century. Many important applications of non-Newtonian fluids are observed in the biological systems, industrial point of view, food industries, chemical and mechanical processes and pharmaceuticals applications. Glass blowing, fiber coating, petroleum, blood, engine oils, greases are referred to the importance of non-Newtonian materials. However, it is noticed that the nature and behavior of such non-Newtonian is not so simple and different in various situations. This critical issue is addressed by presenting various types of non-Newtonian models with different rheology. The micropolar fluid is classified amongst the subcategory of non-Newtonian fluid which predicts the properties at both microscopic and nanoscales structure. The results for couple stress and linear model are retained from micropolar fluid. The fundamental mathematical structure of micropolar fluid was presented by Eringen.[23,24] Some dynamic work on flow of micropolar fluid and other fluid flow can be seen in Refs. 25–35.

This paper addresses the research on bioconvection flow of generalized micropolar nanofluid supporting the bioconvection phenomenon over a uniformly stretched surface. The generalized micropolar fluid predicts the micropolar fluid and viscoelastic properties. The generalized micropolar is the combination of micropolar and second grade fluid. The higher order slip expressions are imposed to the formulated flow problem. The thermal radiative relations and activation energy relations are intended the heat and concentration equations. The consideration of motile microorganisms effectively guaranteed the stability of nanomaterials. The associated laws are used to address the flow equations. The numerical solution is computed via shooting technique with effective accuracy.

2. Problem Statement

Let us consider a 2D bioconvective flow of electrically conducting Micropolar nanofluid over the stretching sheet. The arbitrary motion of the nanoparticles is effectively controlled upon the inclusion of the swimming microorganisms within the fluid. The assumed flow is highly slipping with $u = u_\omega + u_{\text{slip}}$ as a velocity of the stretching sheet. The cartesian coordinate system is selected so that x-axis is along the surface of the sheet, whereas y-axis is normal to it. The flow of fluid and heat, as well as mass transfer, are considered in a steady-state, which is incompressible, laminar and stable. A uniform magnetic field of strength B_0 is imposed perpendicularly with the assumption of a small magnetic Reynolds number such that the induced magnetic field can be ignored. The Buongiorno nanofluid model is utilized in the presence of nonlinear radiation and activation energy to model the temperature and concentration equations. With the help of constant temperature T_w, concentration c_w and density of microorganisms, n_w the fluid is maintained at the surface. At the same time, the fluid that is exterior to the boundary layer is placed at uniform ambient temperature T_∞, concentration c_∞ and the density of microorganisms n_∞ with $T_w, c_w, n_w > T_\infty, c_\infty, n_\infty$. Therefore, upon considering these assumptions, the governing PDEs are written as[27–29]:

$$\frac{\partial v}{\partial y} + \frac{\partial u}{\partial x} = 0, \tag{1}$$

$$v\frac{\partial u}{\partial y} + u\frac{\partial u}{\partial x} + \lambda_0 \left[v\frac{\partial^3 u}{\partial y^3} + \frac{\partial u}{\partial x}\frac{\partial^2 u}{\partial y^2} + \frac{\partial u}{\partial y}\frac{\partial^2 v}{\partial y^2} + u\frac{\partial^3 u}{\partial x \partial y^2} \right]$$

$$= \left(v + \frac{k_1}{\rho_f} \right) \frac{\partial^2 u}{\partial y^2} + \frac{\lambda_1}{\rho_f}\frac{\partial N}{\partial y} - \frac{\sigma_M B_0^2}{\rho_f}u + \frac{1}{\rho_f}[(1 - C_\infty)\rho_f \Lambda g(T - T_\infty)$$

$$- (\rho_p - \rho_f)g(c - c_\infty) - (n - n_\infty)g\gamma^*(\rho_m - \rho_f)], \tag{2}$$

$$v\frac{\partial N}{\partial y} + u\frac{\partial N}{\partial x} = \frac{\gamma}{\rho_f j}\frac{\partial^2 N}{\partial y^2} - \frac{\lambda_1}{\rho_f j}\left(2N + \frac{\partial u}{\partial y} \right), \tag{3}$$

$$u\frac{\partial T}{\partial x} + v\frac{\partial T}{\partial y} = \alpha^\otimes \frac{\partial^2 T}{\partial y^2} + \frac{16\sigma^\otimes}{3(\rho c)_f k^\otimes}\frac{\partial}{\partial y}\left(T^3 \frac{\partial T}{\partial y} \right)$$

$$+ \delta^\oplus \left\{ \frac{D_T}{T_\infty}\left(\frac{\partial T}{\partial y} \right)^2 + D_B \frac{\partial T}{\partial y}\left(\frac{\partial C}{\partial y} \right) \right\}, \tag{4}$$

$$u\frac{\partial c}{\partial x} + v\frac{\partial c}{\partial y} = D_B \frac{\partial^2 c}{\partial y^2} + \frac{D_T}{T_\infty}\frac{\partial^2 T}{\partial y^2} - k_r^2(c - c_\infty)\left(\frac{T}{T_\infty} \right)^n \exp\left(\frac{-E^*}{\kappa T} \right), \tag{5}$$

$$u\frac{\partial n}{\partial x} + v\frac{\partial n}{\partial y} = D_m \frac{\partial^2 n}{\partial y^2} - \frac{b^* w^*}{(c_w - c_\infty)}\frac{\partial}{\partial y}\left(n\frac{\partial c}{\partial y} \right). \tag{6}$$

The velocity components u and v are being oriented along the direction of x-axis and y-axis, respectively. The physical parameters are viscoelastic parameter λ_0, material parameter λ_1, electrical conductivity σ_M, kinematic viscosity ν, fluid density

ρ_f, micro-inertia j, volume suspension coefficient Λ, gravity g, motile density ρ_m, nanomaterials density ρ_p, spin-gradient viscosity γ, thermal diffusivity $\alpha^\otimes$, mean absorption $k^\otimes$, Stefan Boltzmann constant $\sigma^\otimes$, $\delta^\oplus = (\rho c)_p/(\rho c)_f$ nanomaterials heat capacity to fluid heat capacity ratio, diffusion constant D_B, thermophoretic-diffusion D_T, Boltzmann constant κ, activation energy E^*, chemotaxis constant b^*, swimming cells speed w^* and microorganisms diffusion constant D_m. The flow is assessed by employing the following boundary conditions:

$$u = u_\omega + u_{\text{slip}}, \quad v = 0, \quad N = -n_0 \frac{\partial u}{\partial y},$$

$$T = T_w, \quad c = c_w, \quad n = n_w \quad \text{when } y = 0, \tag{7}$$

$$u \to 0, \quad \frac{\partial u}{\partial y} \to 0, \quad N \to 0, \quad T \to T_\infty,$$

$$C \to C_\infty, \quad n \to n_\infty \quad \text{at } y \to \infty, \tag{8}$$

where n_0 reflects the boundary parameter which lies between $0 \le n_0 \le 1$. It is emphasized that $n_0 = 1$ and $n_0 = 0$ represent the turbulent boundary layer flow and concentrated micropolar liquid, respectively.

The higher-order slip relations are introduced:

$$u_{\text{slip}} = \frac{2}{3} \left(\frac{3 - \alpha l^2}{\alpha} - \frac{3}{2} \frac{1 - l^2}{K_n} \right) \beta \frac{\partial u}{\partial y}$$

$$- \frac{1}{4} \left[l^4 + \frac{2}{K_n^2}(1 - l^2) \right] \beta^2 \frac{\partial}{\partial y} \left(\frac{\partial u}{\partial y} - r_0 N \right), \tag{9}$$

$$u_{\text{slip}} = A \frac{\partial u}{\partial y} + B \frac{\partial}{\partial y} \left(\frac{\partial u}{\partial y} - r_0 N \right),$$

where K_n is Knudsen number, β a free path with molecular mean, (A, B) constant while α is momentum coefficient.

The dimensionless form is achieved with proper utilization of the following quantities:

$$\psi = -\sqrt{a\nu x} f(\xi), \quad N = -\sqrt{\frac{a}{\nu}} axg(\xi), \quad \xi = \sqrt{\frac{a}{\nu}} y, \tag{10}$$

$$\theta(\xi) = \frac{T - T_\infty}{T_w - T_\infty}, \quad \phi(\xi) = \frac{c - c_\infty}{c_w - c_\infty}, \quad n(\xi) = \frac{n - n_\infty}{n_w - n_\infty}. \tag{11}$$

The set of formulated problem in view of the above variables is

$$(1 + \Gamma)f''' + ff'' + \Gamma g' - (f')^2 - Mf' - k[-(f'')^2$$

$$+ 2f'f''' - ff''''] + \lambda(\theta - \text{Nr}\varphi - \text{Rb}\chi) = 0, \tag{12}$$

$$\left(1 + \frac{\Gamma}{2}\right) g'' - \Gamma(f'' + 2g) - f'g + g'f = 0, \tag{13}$$

$$\left[1 + \frac{4}{3}\mathrm{Rd}\{1 + (\theta_w - 1)\theta\}^3\right]\theta'' + 4\mathrm{Rd}(\theta_w - 1)[1 + (\theta_w - 1)\theta]^2\theta'^2$$

$$+ \Pr[f\theta' + N_b\theta'\phi' + N_t(\theta')^2] = 0, \tag{14}$$

$$\phi'' + \left(\frac{N_t}{N_b}\right)\theta'' + \mathrm{Sc}f\phi' - \mathrm{Sc}\sigma^{**}(1 + \delta\theta)^n\phi\exp\left(-\frac{E}{1 + \delta\theta}\right) = 0, \tag{15}$$

$$\chi'' + \mathrm{Lb}f\chi' - \mathrm{Pe}(\phi''(\chi + \overline{\omega}) + \chi'\theta') = 0 \tag{16}$$

with boundary conditions:

$$f(0) = 0, \quad f'(0) = 1 + \gamma f''(0) + bf'''(0) + r_0 g'(0),$$
$$g = -n_0 f'', \quad \theta(0) = 1, \quad \phi(0) = 1, \quad \chi(0) = 1, \tag{17}$$

$$f'(\infty) \to 0, \quad f''(\infty) \to 0, \quad g(\infty) \to 0,$$
$$\theta(\infty) \to 0, \quad \phi(\infty) \to 0, \quad \chi(\infty) \to 0, \tag{18}$$

$$M = \sqrt{\sigma_M B_0^2 / \rho_f a}, \quad k = a\lambda_0/\nu, \quad \Gamma = \lambda_1/\rho_f\nu,$$

$$\lambda = \Lambda g(1 - c_\infty)(T_w - T_\infty)/a^2 x,$$

$$\mathrm{Rb} = \gamma^*(n_w - n_\infty)(\rho_m - \rho_f)/\Lambda\rho_f(1 - c_\infty)(T_w - T_\infty),$$

$$\mathrm{Nr} = (\rho_p - \rho_f)(c_w - c_\infty)/\Lambda\rho_f(1 - c_\infty)T_\infty, \quad \Pr(= \nu/\alpha^\otimes),$$

$$\mathrm{Rd} = 4\sigma^\otimes T_\infty^3/3kk^\otimes, \quad N_b = (\rho c)_p D_B(C_w - C_\infty)/(\rho c)_f\nu,$$

$$N_t(= (\rho c)_p D_T(T_w - T_\infty)/(\rho c)_f T_\infty\nu),$$

$$\mathrm{Sc} = \nu/D_B, \quad E = E^*/\kappa T_\infty, \quad \mathrm{Pe} = b^* w^*/D_m,$$

$$\mathrm{Lb} = \nu/D_m.$$

The mathematical relation for wall shear stress is

$$C_f = \frac{\tau_w}{\rho_f u_w^2}, \quad \tau_w = \left[(\mu + \lambda_1)\frac{\partial u}{\partial y} + \lambda_1 N\right]_{y=0}, \quad C_f\sqrt{\mathrm{Re}_x} = (1 + \Gamma)f''(0). \tag{19}$$

Moreover, for wall couple stress force:

$$M_x = \frac{\gamma\left(\frac{\partial N}{\partial y}\right)_{y=0}}{\rho_f a^2 x^3}, \quad M_x\sqrt{\mathrm{Re}_x} = \Gamma G g'(0). \tag{20}$$

The non-dimensional form of local Nusselt number is

$$\frac{\mathrm{Nu_x}}{\sqrt{\mathrm{Re}_x}} = -\left[1 + \frac{4}{3}\mathrm{Rd}(\theta_w - 1)\theta(0) + 1)^3\right]\theta'(0). \tag{21}$$

Similarly, local Sherwood number in non-dimensional form is represented as

$$\frac{\mathrm{Nn}_x}{\sqrt{\mathrm{Re}_x}} = -\chi'(0). \tag{22}$$

3. Solution Methodology

The shooting method is adopted to determine the numerical solution of the ODEs (12)–(16) subject to (17)–(18). The shooting method is useful and easy to implement in software like Matlab due to its low convergence cast and higher accuracy rate. The solution methodology of the shooting method is as follows:

The boundary value problem (BVP) can be transformed into an initial value problem (IVP) upon making the following assumption:

$$f = y_1, \quad f' = y_2, \quad f'' = y_3, \quad f''' = y_4, \quad g = y_5, \quad g' = y_6,$$
$$\theta = y_7, \quad \theta' = y_8, \quad \phi' = y_{10}, \quad \chi = y_{11}, \quad \chi' = y_{12}. \tag{23}$$

The assumptions (13) implies the transformation of BVP (12)–(16) into IVP as follows:

$$y_1' = y_2,$$
$$y_2' = y_3,$$
$$y_3' = y_4,$$
$$y_4' = -\frac{(1+\Gamma)y_4 + y_1 y_{3+\Gamma y_6} = y_2^2 = My_2 - k(-y_3^2 + 2y_2 y_4) + \lambda(y_7 - \text{Nr}y_9 - \text{Rb}y_{11})}{ky_1},$$
$$y_5' = y_6,$$
$$y_6' = -\frac{-\Gamma(y_3 + 2y_5) - y_2 y_5 + y_6 y_1}{\left(1 + \frac{\Gamma}{2}\right)}, \tag{24}$$
$$y_7' = y_8,$$
$$y_8' = -\frac{4\text{Rd}(\theta_w - 1)(1 + (\theta_w - 1)y_7)^2 y_8^2 + \text{Pr}(y_1 y_8 + N_b y_8 y_{10} + N_t y_8^2)}{\left(1 + \frac{4}{3}\text{Rd}(1 + (\theta_w - 1)y_7)^3\right)},$$
$$y_9' = y_{10},$$
$$y_{10}' = -\left(\left(\frac{N_t}{N_b}\right)y_8' + \text{Sc}y_1 y_{10} - \text{Sc}\sigma^{**}(1 + \delta y_7)^n y_9 \exp\left(-\frac{E}{1 + \delta y_7}\right)\right),$$
$$y_{11}' = y_{12},$$
$$y_{12}' = -(\text{Lb}y_1 y_{12} - \text{Pe}(y_{10}'(y_{11} + \overline{\omega}) + y_{12}y_{10})).$$

The boundary conditions are transformed to:

$$y_1(0) = 0, \quad y_2(0) = 1 + \gamma y_3(0) + b y_4(0) + r_0 y_6(0), \quad y_3(0) = a_1,$$
$$y_4(0) = a_2, \quad y_6(0) = a_3, \quad y_5(0) = -n_0 y_3(0), \quad y_7(0) = 1, \tag{25}$$
$$y_8(0) = a_4, \quad y_9(0) = 1, \quad y_{10}(0) = a_5, \quad y_{11}(0) = 1, \quad y_{12}(0) = a_6,$$

$$y_2(\infty) \to 0, \quad y_3(\infty) \to 0, \quad y_5(\infty) \to 0, \quad y_7(\infty) \to 0,$$
$$y_9(\infty) \to 0, \quad y_{11}(\infty) \to 0. \tag{26}$$

in which a_1, a_2, a_3, a_4, a_5 and a_6 are the missing initial conditions.

Further, the value of ξ can be chosen between 1 to 10, and the values of missing initial conditions are chosen arbitrarily, i.e., $a_1 = a_2 = a_3 = a_4 = a_5 = a_6 = 1$. Then, the fourth-fifth order RK-Method can be used to solve the ODEs. Finally, the values of missing initial conditions can be validated through Newton's method to achieve the required accuracy.

4. Results and Discussion

The impacts of governing parameters upon the non-dimensional distributions of the velocity $f'(\xi)$, microrotation velocity $g(\xi)$, temperature $\theta(\xi)$, concentration $\phi(\xi)$ and microorganisms $\chi(\xi)$ are examined graphically. The physical quantities of interest like local Nusselt number and local density number are also calculated.

4.1. *Velocity profiles*

The effects of the magnetic parameter M and vortex viscosity parameter Γ upon the non-dimensional velocity $f'(\xi)$ and microrotation $g(\xi)$ profiles are presented in Figs. 1–4. A comparison is made when viscoelastic parameter $k = 0.1$ and $k = 0.5$ along with non-dimensional similarity variable ξ. The upshots of M upon $f'(\xi)$ and $g(\xi)$ are depicted in Figs. 1 and 2. From these figures, it is noticed that the velocity $f'(\xi)$ and microrotation $g(\xi)$ profiles are decaying along with ξ for higher estimations of the magnetic parameter M. Both profiles have attained their maximum values when $M = 0$ whereas for $M \neq 0$ the profiles are gradually decreasing. The increases in the magnetic parameter lead to the Lorentz force's existence in the electrically conducting fluid, which opposes the fluid's motion. As a result, velocity and microrotation profiles reduce. It is further noticed that the reduction in the
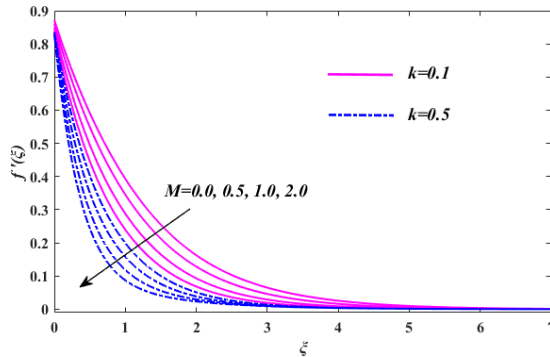

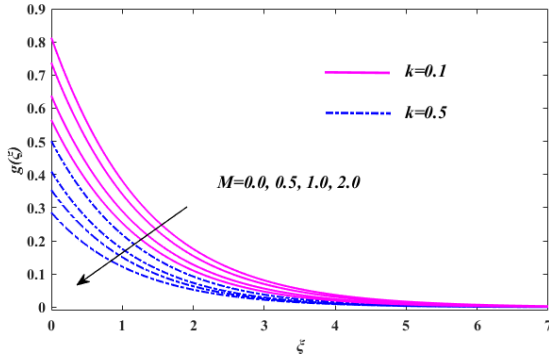Fig. 1.   (Color online) Effects of M upon $F'(\xi)$.

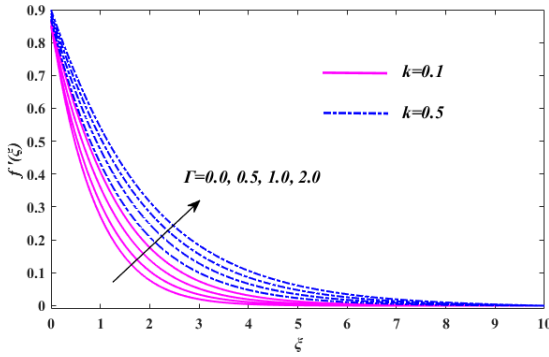Fig. 2.   (Color online) Effects of M upon $G(\xi)$.

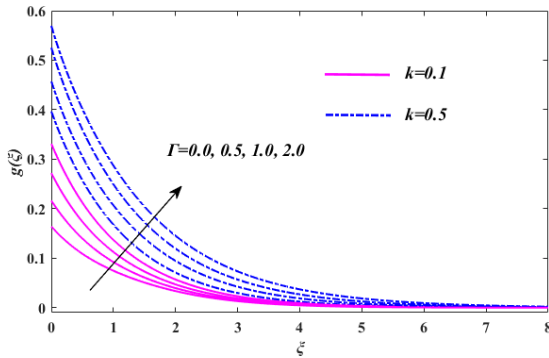Fig. 3.   (Color online) Effects of Γ upon $F'(\xi)$.

Fig. 4.   (Color online) Effects of Γ upon $G(\xi)$.

boundary layer for $k = 0.5$ is on a higher note than from $k = 0.1$. The influences of the Γ upon $f'(\xi)$ and $g(\xi)$ are elucidated in Figs. 3 and 4. Both profiles escalates along ξ as vortex viscosity parameter Γ rises. The value of both profiles is minimum in the absence of a vortex viscosity parameter, i.e., $\Gamma = 0$. Physically, the higher

estimations of the vortex viscosity parameter cause the lower viscosity due to which the velocity $f'(\xi)$ and microrotation $g(\xi)$ profiles escalate. Also, the thickness of the boundary layer is thicker for $k = 0.5$ than from $k = 0.1$.

4.2. *Temperature profiles*

The effects of the radiation parameter Rd, surface heating parameter θ_w, Prandtl number Pr, Brownian motion parameter N_b and Thermophoresis parameter N_t upon the non-dimensional profiles of temperature $\theta(\xi)$ are encapsulated in Figs. 5–9. Figure 5 shows the impression of the parametert Rd upon $\theta(\xi)$. The temperature profile is increasing along ξ for rising values of the radiation parameter Rd. The concept behind this is that the increase in the radiation parameter causes the reduction in the mean absorption coefficient due to which further heat is delivered towards the direction of the fluid and as a result temperature increases. The increase in the temperature is on higher notes for $k = 0.5$. Figure 6 deals to observe the upshots of the parameter θ_w upon $\theta(\xi)$. The temperature $\theta(\xi)$ is observed escalating along for rising values of the surface heating parameter θ_w. It is noted that $\theta_w = 1$ means the
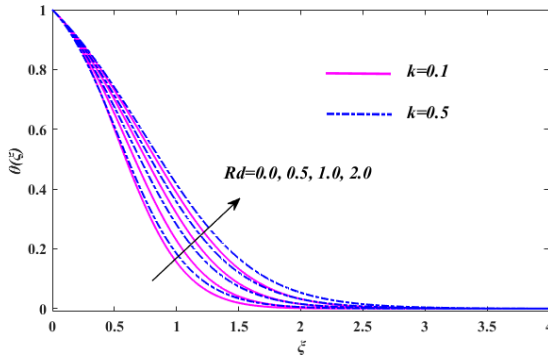

Fig. 5.   (Color online) Effects of Rd upon $\theta(\xi)$.
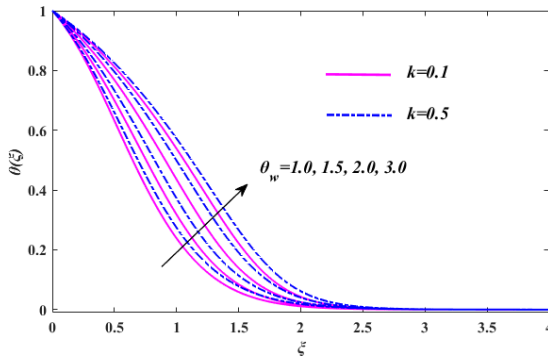

Fig. 6.   (Color online) Effects of θ_w upon $\theta(\xi)$.
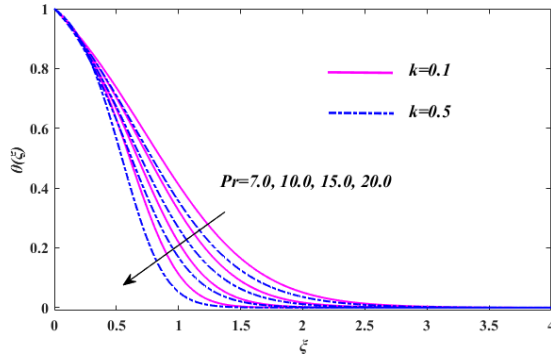
Fig. 7.   (Color online) Effects of Pr upon $\theta(\xi)$.
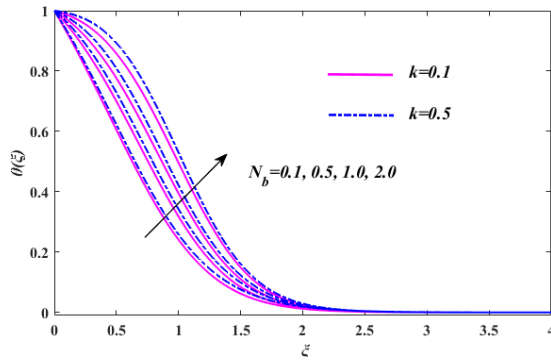

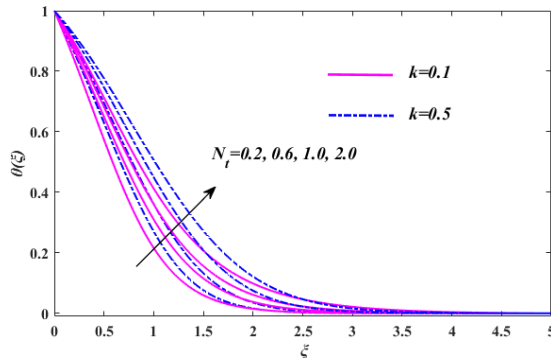Fig. 8.   (Color online) Effects of N_b upon $\theta(\xi)$.

Fig. 9.   (Color online) Effects of N_t upon $\theta(\xi)$.

linear radiation and $\theta_w > 1$ implies the nonlinear radiation. The escalation in the surface heating parameter leads to a more extensive fluid temperature than from the ambient temperature, because of which the thermal state of the temperature is increased and as a result temperature enhances. The escalation in the profile of

temperature is a little higher for $k = 0.5$. Figure 7 portrays the effects of the parameter Pr upon $\theta(\xi)$. It is examined in Fig. 7 that the temperature and boundary layer thickness decreases as the Prandtl number enhances Pr. Because the Prandtl number is mainly associated with thermal and momentum diffusivities; therefore, the rise in the Prandtl number causes the dominance of momentum diffusivity over thermal diffusivity because of which the temperature decays. The reduction in the behaviour of the temperature and boundary layer is more considerable for $k = 0.5$. The impact of the parameter N_b upon $\theta(\xi)$ is captured in Fig. 8. The temperature $\theta(\xi)$ is enhancing along ξ for growing values of the Brownian motion parameter N_b. During the Brownian motion process, the arbitrary motion of the fluid particles is enabled because of which additional heat energy is generated and as a result temperature enhances. The enhancement in the temperature is more extensive for $k = 0.5$ than from $k = 0.1$. The profile of the temperature $\theta(\xi)$ in Fig. 9 is observed increasing along ξ for growing values of the thermophoresis parameter N_t. In the thermophoresis phenomenon, the fluid particles are dragged back from warm to the cold surface due to which temperature escalates. Also, the boundary layer thickness increases and this increase in the case of $k = 0.5$ is higher than from $k = 0.1$.

4.3. *Concentration profiles*

The effects of the Brownian motion parameter N_b and Thermophoresis parameter N_t, Schmidt number Sc and activation energy parameter E upon the concentration distribution $\phi(\xi)$ are demonstrated in Figs. 10–13. The concentration profile $\phi(\xi)$ in Fig. 10 is seen decaying along ξ for growing values of the Brownian motion parameter N_b. The collision of the nanoparticles during the Brownian motion process produces the resistance due to which concentration reduces. The reduction in the concentration of nanoparticles is on a higher note in the case of $k = 0.5$ than from $k = 0.1$. The effects of the parameter N_t upon $\phi(\xi)$ are provided in Fig. 11. It is noticed that the concentration is increasing along ξ for rising values of the thermophoresis parameter N_t. The number of nanoparticles is increased during the
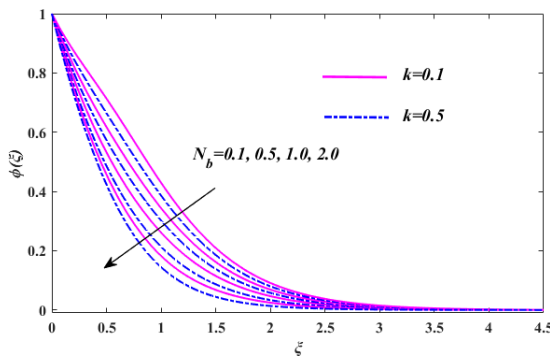

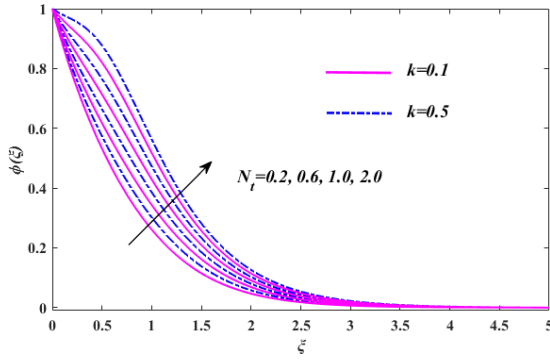Fig. 10.   (Color online) Effects of N_b upon $\phi(\xi)$.

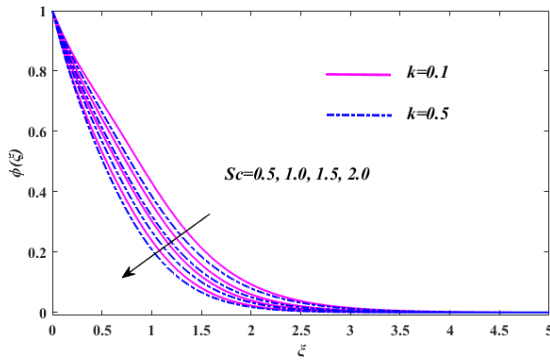Fig. 11.   (Color online) Effects of N_t upon $\phi(\xi)$.

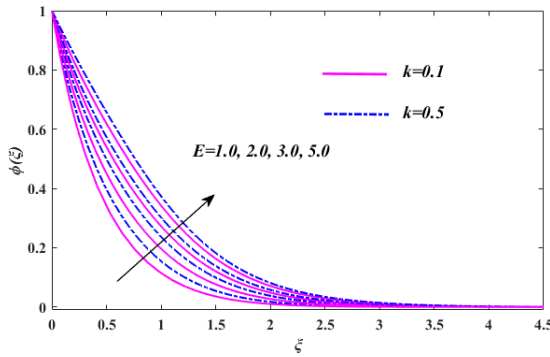Fig. 12.   (Color online) Effects of Sc upon $\phi(\xi)$.

Fig. 13.   (Color online) Effects of E upon $\phi(\xi)$.

thermophoresis because of which the concentration of the nanoparticles enhances. The enhancement for $k = 0.5$ is more extensive. The effects of the parameter Sc upon $\phi(\xi)$ are displayed in Fig. 12. The concentration profile in Fig. 12 is decaying along ξ for higher values of the Schmidt number Sc. As the Schmidt number is in

an inverse relationship with mass diffusivity, that is why the rise in the Schmidt number owns a weeker mass diffusivity, and as a result, concentration decays. The effects of the parameter E upon $\phi(\xi)$ are reflected in Fig. 13. As it is evident that the increase in the activation energy parameter leads to the rise in the concentration profile. The higher estimation in the activation energy parameter causes a lower reaction rate due to which the chemical reaction decays and as a result concentration enhances. Thus the enhancement for $k = 0.5$ is more extensive.

4.4. *Microorganisms profiles*

The effects of the bioconvection Lewis number Lb, Peclet number Pe and bioconvection parameter $\overline{\omega}$ upon the dimensionless distribution of the microorganisms are depicted in Figs. 14–16. It is examined from these figures that the profile of microorganisms is a decreasing function of the parameters Lb, Pe and $\overline{\omega}$. The diffusivity of the microorganisms decays as the bioconvection Lewis number surges because of which microorganisms enhances. In additions, the increase in the Peclet number
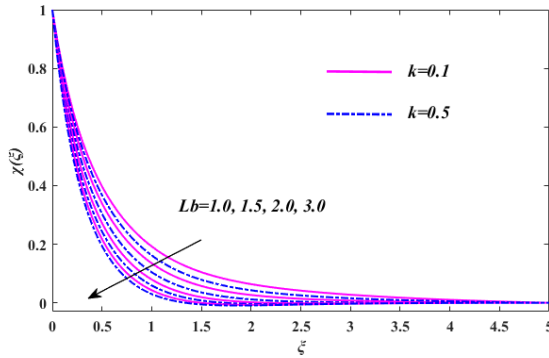

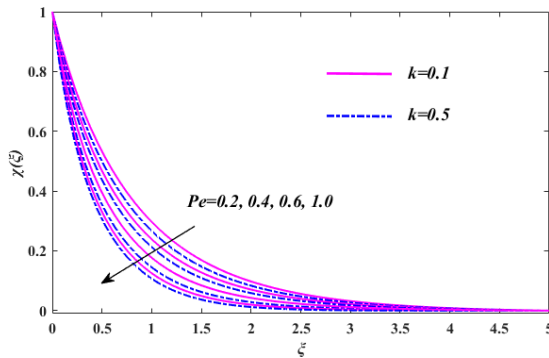Fig. 14.   (Color online) Effects of Lb upon $\chi(\xi)$.

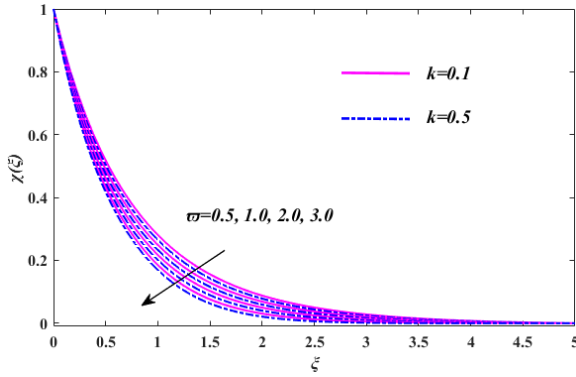Fig. 15.   (Color online) Effects of Pe upon $\chi(\xi)$.

Fig. 16.   (Color online) Effects of $\overline{\omega}$ upon $\chi(\xi)$.

causes the increase in the swimming motion of the self-propelled microorganisms, which is responsible for the increment in concentration profile. Also, the higher estimations of the bioconvection parameter lead to the diminution in the thickness of the boundary layer because of which the microorganisms profile decreases. It is further examined from Figs. 14–16 that the decrease in the concentration profile is slightly higher for $k = 0.5$ than that of $k = 0.1$.

Table 1.   The numerical values of the local Nusselt number.

Γ	Rd	θ_w	Pr	N_b	N_t	$\dfrac{\mathrm{Nu}_x}{\sqrt{\mathrm{Re}_x}}$	
						$k = 0.1$	$k = 0.5$
0.2	0.5	1.5	6.2	0.1	0.2	2.0454	2.0681
0.5						2.0860	2.0891
1.0						2.1362	2.1366
2.0						2.1974	2.1980
0.2	1.0					2.8359	2.8626
	1.5					3.4796	3.5102
	2.0					4.0352	4.0695
	0.5	1.0				1.4332	1.4437
		2.0				2.8626	2.9057
		3.0				4.9179	5.0006
		1.5	7.0			2.1174	2.1440
			10.0			2.3121	2.3551
			15.0			2.4792	2.5517
			6.2	0.5		1.2187	1.2488
				1.0		0.6036	0.6257
				2.0		0.1321	0.1392
				0.1	0.6	1.5015	1.5316
					1.0	1.1441	1.1789
					1.5	0.8559	0.8923
					2.0	0.6716	0.7061

Table 2.   The numerical values of the local density number.

| Γ | Lb | Pe | $\overline{\omega}$ | $\frac{\mathrm{Nn}_x}{\sqrt{\mathrm{Re}_x}}$ | |
				$k = 0.1$	$k = 0.5$
0.2	1.0	0.2	0.3	1.3992	1.3916
0.5				1.4003	1.3956
1.0				1.4022	1.3995
2.0				1.4052	1.4041
0.2	1.5			1.8957	1.8882
	2.0			2.3955	2.3881
	3.0			3.3956	3.3881
	1.0	0.4		1.7922	1.7771
		0.6		2.1856	2.1630
		1.0		2.9735	2.9360
		0.2	0.5	1.4589	1.4500
			1.0	1.6080	1.5959
			2.0	1.9065	1.8883
			3.0	2.2054	2.1812

4.5. *Local Nusselt number*

Table 1 demonstrates the calculated numerical values of the local Nusselt number for various values of the parameters like Γ, Rd, θ_w, Pr, N_b and N_t. The values are calculated in the case when $k = 0.5$ and $k = 0.1$. The other parameters are fixed as $M = 0.5, \lambda = 2, \mathrm{Nr} = 0.1, \mathrm{Rb} = 0.1, \mathrm{Sc} = 2, \sigma^{**} = 1, \delta = 1, n = 1, E = 1, \mathrm{Lb} = 1, \mathrm{Pe} = 0.2, \overline{\omega} = 1.8, \gamma = 0.2, b = 0.5, r_0 = 0.3, n_0 = 0.4$. The local Nusselt get maximum numerical values with Γ and Rd for both $k = 0.1$ and $k = 0.5$. The increasing rate due to these parameters is relatively maximum when $k = 0.5$.

4.6. *Local density number*

Table 2 shows the calculated numerical values of the local density number for different values of the parameters like Γ, Lb, Pe and $\overline{\omega}$. The values are calculated when $k = 0.5$ and $k = 0.1$. The other parameters are fixed. The increasing trend in $\frac{\mathrm{Nn}_x}{\sqrt{\mathrm{Re}_x}}$ is observed for $\overline{\omega}$, Pe and Γ.

5. Conclusions

Present investigation presented the results for flow of modified micropolar nanofluid with addition of motile microorganisms over convectively heated surface. The higher order slip constraints and activation energy features are also accounted to the thermally developed flow. The shooting algorithm with MATLAB software is tested to simulate the numerical data. The graphical inspection of all parameters is intended in view of viscoelastic nature of micropolar fluid. The major findings are listed as

• An increasing change in microrotation velocity due to variation of vortex viscosity is examined which is more effective when value of viscoelastic parameter increases.

- The temperature enhanced for the uplift variation of surface heating, thermophoresis constant and viscoelastic parameter.
- The declining trend for increasing numerical values of Prandtl number is more progressive when the value of viscoelastic parameter increases.
- The presence of activation energy is more effective for enhancing nanofluid concentration.
- The increasing profile of concentration field is more progressive when fluid is more viscous.
- The changes in bioconvection parameter and Peclet number parameter reduce the motile microorganism.

Acknowledgments

References

1. S. U. S. Choi, Enhancing thermal conductivity of fluids with nanoparticles, in *Int. Mechanical Engineering Congress and Exhibition*, ASME, Vol. 66 (1995), pp. 99–105.
2. J. Buongiorno, *J. Heat Transf.* **128**, 240 (2006); M. Turkyilmazoglu, *Comput. Methods Programs Biomed.* **179**, 104997 (2019).
3. M. M. Bhatti *et al.*, *Mod. Phys. Lett. B* **34**, 2050026 (2020).
4. M. Sohail and R. Raza, *Multidiscip. Model. Mater. Struct.* **16**, 1061 (2020).
5. S. U. Khan *et al.*, *Phys. Scr.* **94**, 125211 (2019).
6. L. A. Lund *et al.*, *Symmetry* **12**, 276 (2020).
7. M. Turkyilmazoglu, *Comput. Methods Programs Biomed.* **187**, 105171 (2020).
8. F. Mebarek-Oudina *et al.*, *Int. Commun. Heat Mass Transf.* **117**, 104737 (2020).
9. M. Kumar, K. Pravin Kashyap and N. Naresh Kumar, *SN Appl. Sci.* **848**, 1 (2020).
10. M. Ijaz Khan and F. Alzahrani, *Math. Comput. Simul.* **185**, 47 (2021).
11. Y.-M. Chu *et al.*, *J. Mater. Res. Technol.* **9**, 13977 (2020).
12. A. V. Kuznetsov, *Int. Commun. Heat Mass Transf.* **37**, 1421 (2010).
13. A. V. Kuznetsov, *Nanoscale Res. Lett.* **6**, 100 (2011).
14. F. T. Zohraa *et al.*, *Chin. J. Phys.* **56**, 432 (2018).
15. S. M. Atif, S. Hussain and M. Sagheer, *AIP Adv.* **9**, 025208 (2019).
16. L. Zhang *et al.*, *Appl. Math. Mech. Engl.* **41**, 637 (2020).
17. M. N. Khan *et al.*, *Surf. Interfaces* **21**, 100686 2020.
18. M. Dhlamini *et al.*, *J. Central South Univ.* **27**, 824 (2020).
19. A. Zeeshan *et al.*, *Int. J. Mod. Phys. B* **34**, 2050110 (2020).
20. H. Waqas *et al.*, *Symmetry* **12**, 214 (2020).
21. A. Aldabesh *et al.*, *Alex. Eng. J.* **59**, 4315 (2020).
22. M. Waqas *et al.*, *Appl. Nanosci.* **9**, 1193 (2019).
23. A. C. Eringen, *Int. J. Eng. Sci.* **2**, 205 (1964).
24. A. C. Eringen, *J. Math. Mech.* **16**, 1 (1966).
25. A. C. Eringen, *J. Math. Anal. Appl.* **38**, 480 (1972).
26. S. M. M. El-Kabeir, *Can. J. Phys.* **83**, 1007 (2005), doi:10.1139/p05-039.
27. Z. Abbas, M. Sheikh and M. Sajid, *Can. J. Phys.* **92**, 1 (2014), doi:10.1139/cjp-2013-0329.

28. H. A. Nabwey and A. Mahdy, *Alex. Eng. J.* **60**, 1739 (2021).
29. E. O. Fatunmbi and S. O. Salawu, *Propuls. Power Res.* **9**, 281 (2020).
30. M. M. Khader and R. Prakash Sharma, *Math. Comput. Simul.* **181**, 333 (2021).
31. B. Shankar Goud, *Int. J. Thermofluids* **7−8**, 100044 (2020).
32. S. Nadeem, M. N. Khan and N. Abbas, *Alex. Eng. J.* **59**, 3443 (2020).
33. M. I. Khan and F. Alzahrani, *Math. Comput. Simul.* **185**, 47 (2021).
34. M. I. Khan and F. Alzahrani, *Int. J. Hydrog. Energy* **46**, 1362 (2020).
35. M. I. Khan *et al.*, *Surf. Interfaces* **22**, 100849 (2021).
36. M. Nazeer *et al.*, *Surf. Interfaces* **22**, 100846 (2021).
37. Y. M. Chu *et al.*, *Alex. Eng. J.* **60**, 1851 (2021).